Annual Review of Biochemistry

The Structural Dynamics of Translation

Andrei A. Korostelev

RNA Therapeutics Institute, University of Massachusetts Chan Medical School, Worcester, Massachusetts, USA; email: andrei.korostelev@umassmed.edu

Annu. Rev. Biochem. 2022. 91:3.1–3.23

The *Annual Review of Biochemistry* is online at biochem.annualreviews.org

https://doi.org/10.1146/annurev-biochem-071921-122857

Keywords

Cryo-EM, ribosome, RNA dynamics, translation initiation, translation elongation, translation termination

Abstract

Accurate protein synthesis (translation) relies on translation factors that rectify ribosome fluctuations into a unidirectional process. Understanding this process requires structural characterization of the ribosome and translation-factor dynamics. In the 2000s, crystallographic studies determined high-resolution structures of ribosomes stalled with translation factors, providing a starting point for visualizing translation. Recent progress in single-particle cryogenic electron microscopy (cryo-EM) has enabled near-atomic resolution of numerous structures sampled in heterogeneous complexes (ensembles). Ensemble and time-resolved cryo-EM have now revealed unprecedented views of ribosome transitions in the three principal stages of translation: initiation, elongation, and termination. This review focuses on how translation factors help achieve high accuracy and efficiency of translation by monitoring distinct ribosome conformations and by differentially shifting the equilibria of ribosome rearrangements for cognate and near-cognate substrates.

Contents

1. INTRODUCTION: THE ACCURACY OF TRANSLATION AND GLOBAL RIBOSOME REARRANGEMENTS

The fidelity of protein synthesis (translation) depends on accurate initiation and sequential addition of amino acids to a polypeptide chain until the ribosome reaches the stop codon of the open reading frame of a messenger RNA (mRNA). At each stage of translation—initiation, elongation, or termination—the ribosome must collaborate with the appropriate substrates: tRNA or translation factor protein. The correct substrates do not form an orderly queue, awaiting their turn on the ribosome. Rather, the ribosome randomly encounters substrates and quickly decides to accept or reject them while establishing and maintaining the reading frame. How does the ribosome select the correct tRNA or translation factor at each stage of translation, and how does the correct selection of substrates drive translation? The process depends in large part on the conformational dynamics of the ribosome.

The ribosome consists of the large and small subunits, each containing three tRNA binding sites (**Figure 1*a–c***). Mobility of the small ribosomal subunit was predicted half a century ago to underlie translation (1). Early structural studies of the bacterial 70S and eukaryotic 80S ribosomes captured four large-scale rearrangements of the small subunit (**Figure 1*d***). The two most extensive rearrangements include a ∼10° rotation of the small subunit relative to the large subunit (known as intersubunit rotation or body rotation) and a ∼20° rotation of the head of the small subunit relative to its body (known as head swivel) (**Figure 1*d***). Both rearrangements were initially associated with the translocation of tRNAs and mRNA (2–4), consistent with solution fluorescence studies, such as Förster resonance energy transfer (FRET) (5–7). After peptidyl transfer from peptidyl-tRNA in the P site to aminoacyl-tRNA (aa-tRNA) in the A site, forward (also termed counterclockwise) (**Figure 1*d***) rotation of the small subunit is coupled with movement of the tRNA acceptor arms on the large subunit (**Figure 1*a*,*b***). This results in a rotated ribosome with hybrid tRNA states—e.g., A/P tRNA with the anticodon stem loop (ASL) in the A site of the small subunit and the acceptor arm in the P site of the large subunit (**Figure 1*b***). The first part of the name of hybrid or chimeric tRNA states, such as A/P or ap/P, denotes the position of the ASL on the small subunit, the last letter denotes the position of the acceptor arm on the large subunit (for more details on this nomenclature, see **Table 1**). In the presence of translocase elongation factor G (EF-G), reverse (clockwise) rotation propels the ASLs of the A- and P-site tRNAs on the small subunit to the P and E (exit) sites, respectively (**Figure 1*c***) (8). During reverse rotation, the head domain of the

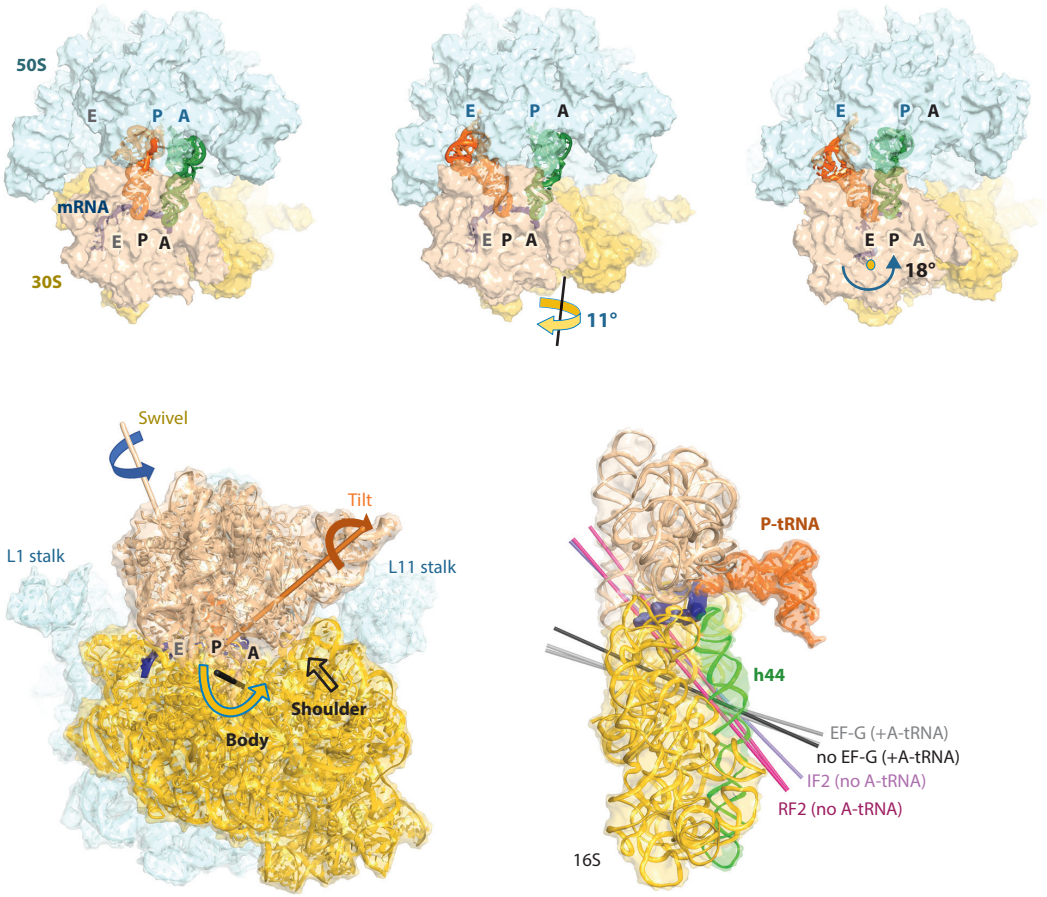

Figure 1

Structure of the bacterial ribosome and large-scale 30S rearrangements. (*a*) Pretranslocation nonrotated 70S with the classical peptidyl-tRNA (*green*) and deacyl-tRNA (*orange*) in the P and A sites, respectively, observed without translation factor proteins. The tRNA-binding A, P, and E sites are labeled. (*b*) Pretranslocation 70S with hybrid-state P/E and A/P tRNAs with a fully rotated 30S body (10–11° relative to the nonrotated ribosome shown in panel *a*, as indicated by the arrow) and slightly swiveled 30S head (3–4°; not shown), observed without translation factor proteins. (*c*) 70S ribosome with nearly translocated chimeric ap/P and pe/E tRNAs (see Section 3) with a partially rotated 30S body (~4°; not shown) and highly swiveled 30S head (18°; indicated by arrow), observed without translation factor proteins (102) (*d*) Solvent side of the small ribosomal subunit, showing the four principal rearrangements: head swivel (*beige axis*), head tilt (*orange axis*), body rotation (*black axis*), and shoulder movement (*black outlined arrow*). Arrows denote the directions of forward rotation (*curved*) and shift (*straight*). (*e*) Axes of intersubunit body rotation in 70S complexes show similar pivot points (near residues 1,420–1,425 of 16S helix 44) for 30S body rotation without protein factors (*black*), with IF2 (*violet*), with EF-G (*gray*), and with RF2 (*magenta*). Two gray and two magenta arrows are derived from complexes obtained in different studies. The 50S subunit and ribosomal proteins are not shown. The 30S head and body are shown in beige and yellow, respectively, in all panels. The degrees of intersubunit rotation were measured relative to the previously published nonrotated posttranslocation 70S structure VII (97). Abbreviations: EF, elongation factor; IF, initiation factor; RF, release factor; tRNA, transfer RNA.

small subunit swivels toward the large subunit (forward head swivel), enabling tRNA translocation relative to the body (3). Observed in vacant ribosome crystal structures, head swivel is an inherent ribosomal rearrangement that was proposed to facilitate translocation of deacyl-tRNA by widening a gate between the P and E sites (4). Reverse swivel completes the translocation cycle, restoring the ribosome to a nonrotated conformation, ready to accept the next aa-tRNA. Notably, structural

Table 1 Nomenclature for ribosomal positions of tRNA[a]

tRNA	Aminoacylation status	Position in ribosome structure
Classical states (observed predominantly on the nonrotated ribosome)		
A (also termed A/A)[b]	Aminoacyl or peptidyl	ASL and CCA are both in the A sites of the small and large subunits. (This state can also be sampled on the rotated ribosome)
P (also termed P/P)	Peptidyl or deacyl (or aminoacyl during initiation)	ASL and CCA are both in the P sites of the small and large subunits.
E (also termed E/E)	Deacyl	ASL and CCA are both in the E sites of the small and large subunits.
Hybrid states (observed predominantly on the fully rotated ribosome)		
A/P	Peptidyl	ASL is in the A site of the small subunit. CCA is in the P site of the large subunit.
A/P*	Peptidyl	ASL is in the A site of the small subunit. CCA is in the P site of the large subunit. The elbow of tRNA is shifted ~20 Å toward the P site relative to that in the A/P state.
P/E	Deacyl	ASL is in the P site of the small subunit. CCA is in the E site of the large subunit.
Chimeric states (observed predominantly on the partially rotated ribosome)		
ap/P	Peptidyl	ASL interacts with A-site elements of the small-subunit head domain and with P-site elements of the small-subunit body domain. CCA is in the P site of the large subunit.
ap*/P	Peptidyl	ASL interacts with A-site elements of the small-subunit head domain and is shifted ~4 Å further into the P-site of the small-subunit body domain relative to ap/P state. CCA is in the P site of the large subunit.
pe/E	Deacyl	ASL interacts with P-site elements of the small-subunit head domain and with E-site elements of the small-subunit body domain. CCA is in the E site of the large subunit.

Abbreviations: ASL, anticodon stem loop; CCA, 3′ terminal cytidine, cytidine, adenosine.

[a]Alternative nomenclatures (such as A/ap, PRE1, CHI, or INT1) are used based on biophysical observations (e.g., see 64, 93, 151).

[b]The first part of the name denotes the position of the ASL on the small subunit; the last letter denotes the position of the acceptor arm on the large subunit.

and biophysical studies revealed that the small subunit spontaneously rotates in the absence of EF-G (5) and that rotations coincide with tRNA fluctuations within the ribosome (9), suggesting that they are inherent and thermally driven movements. Spontaneous rotation, however, is futile and does not result in efficient translocation without EF-G.

Two smaller 30S-domain movements identified by early cryogenic electron microscopy (cryo-EM) and X-ray studies were ascribed to translation fidelity. Head tilt, in which the head domain of the small subunit rotates about an axis roughly perpendicular to that of head swivel, brings the head closer to the large 50S subunit (**Figure 1*d***). Head tilt has been observed on the isolated small subunit in the absence (10) and presence of initiator tRNA (11), suggesting that this inherent movement is important for the recognition of initiator tRNA during initiation. Shoulder movement, also termed domain closure, was identified by comparing crystal structures formed with and

without tRNA ASLs used to mimic tRNAs; this movement was proposed to underlie the fidelity of mRNA decoding (12).

Single-state ribosome complexes from early X-ray crystallography and cryo-EM studies provided important insights into different ribosome conformations. Nevertheless, key structural intermediates have been missing that could explain how the ribosomes and translation factors regulate translation fidelity. For example, crystal structures of ribosomes with cognate tRNA (complementary to the paired mRNA codon) or near-cognate tRNA (anticodon with one noncomplementary nucleotide) revealed markedly similar interactions (13, 14), even though near-cognate tRNAs are efficiently rejected by the ribosome in cellular and biochemical studies. Furthermore, structural studies have relied on the use of inhibitors, mutations, or GTP analogs to capture complexes with translation factors, such as the essential translational GTPases. These complexes might capture off-pathway intermediates and/or fail to visualize the conformations essential for function.

Recent advances in cryo-EM have helped to bridge these gaps by enabling near-atomic structure determination of complexes formed under conditions that mimic authentic translation. Improved data quality and computational approaches now allow high-resolution differences to be resolved within an ensemble of structures from a single sample. Moreover, time-resolved cryo-EM approaches allow temporal separation and capture of transient structural states, including those involved in GTP hydrolysis. Arranging these structures along a reaction trajectory, informed by biochemical and biophysical studies, offers a high-resolution movie-like view of translation steps that had long evaded structural characterization. Recent time-resolved and ensemble cryo-EM studies have revealed that the inherent large-scale inter- and intrasubunit rearrangements are essential at all three stages of translation; these studies also demonstrated how ribosome dynamics collaborate with translation factors to ensure accurate and efficient translation.

This review presents a concise account of recent cryo-EM studies, which allow a more complete structural reconstruction of translation than previously available. The review focuses on the structural mechanisms that explain translation accuracy at all three steps of bacterial translation and draws parallels with eukaryotic translation. The discussion outlines how the inherent ribosome dynamics define the high fidelity of each step. Some local structural elements of the ribosome, which rearrange to assist translation [e.g., the tRNA-binding L1 stalk and factor-binding L11 stalk (P-stalk in eukaryotes) (**Figure 1**)] and eukaryote-specific subunit rolling, are not discussed in detail, as their roles have been discussed elsewhere (e.g., 15–18).

2. INITIATION

To initiate translation, the ribosome must correctly position the mRNA open reading frame. The correct positioning is achieved when the AUG start codon in the P site pairs with the initiator tRNA: formyl-methionyl-tRNA in bacteria (fMet-tRNA^{fMet}, where the prefix denotes the aminoacylation status, and the superscript identifies the tRNA) or methionyl-tRNA in eukaryotes. A wobble pairing in the first nucleotide position of the codon allows infrequent initiation from GUG, UUG, and CUG, whereas other codons are strictly discriminated against (19, 20). The molecular players of initiation have been characterized by decades of research (reviewed in 21, 22). In the bacterial ribosome, the AUG codon is held in the P site by the upstream Shine–Dalgarno sequence (23, 24), which base pairs with the 3′ end of 16S rRNA (25, 26). Dynamic RNA-binding protein S1, upstream from the E site, also contributes to positioning the mRNAs, in particular those with weak or absent Shine–Dalgarno sequences (27). Formation of the 70S initiation complex with initiator tRNA in the P site is aided by initiation factors IF1, IF2, and IF3. Although a bacterial 70S initiation complex can be formed without initiation factors in vitro, the three factors are required for fast and accurate initiation (22, 28).

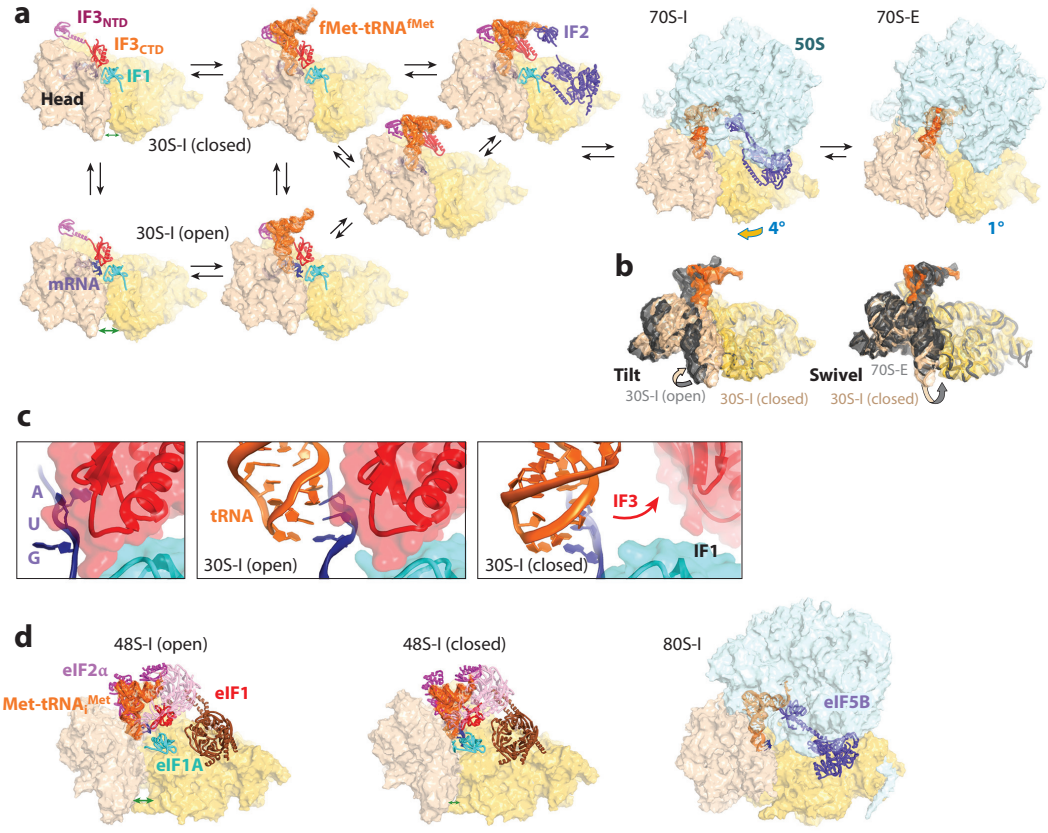

Figure 2

Cryo-EM structures visualize initiation factors and 30S rearrangements underlying the fidelity of initiation. (*a*) Possible trajectories of initiation complex formation derived from ensemble cryo-EM (11) and time-resolved cryo-EM (43) studies. The existence of 30S-I in closed and open conformations in a single sample implies spontaneous rearrangements with different combinations of IF1 and IF3, whereas IF2 binds to 30S-I (closed), sampled upon acceptance of the correct tRNA. Double-ended green arrows indicate mobility of the head due to head tilt, resulting in different distances between the head (*beige*) and body (*yellow*) of the 30S subunit. The degrees of 30S body rotation in two 70S complexes are indicated. (*b*) Superposition of 30S structures shows the head tilt between open and closed 30S-I conformations and head swivel between 30S-I (closed) and 70S-I complexes, along with initiator-tRNA rearrangements. Superposition was performed by the alignment of the body domains of 16S rRNA (residues 930–1,385). Only 16S rRNA is shown for clarity. (*c*) Close-up view of the P site, showing interactions of IF3 (*red*) and IF1 (*cyan*) with mRNA (*blue*) and initiator tRNA (*orange*) in the open and closed 30S-I states, which are implicated in the mechanism of tRNA acceptance (11). (*d*) Cryo-EM structures of the eukaryotic 48S initiation complex reveal that the small-subunit movements and tRNA interactions with initiation factors are overall similar to the bacterial ones, despite large mechanistic and sequence divergence. Initiation factors, whose positions are similar to bacterial release factors, are labeled. The degrees of intersubunit rotation were measured relative to the previously published nonrotated posttranslocation 70S structure VII (96). Protein Data Bank identifiers from left to right: 3jaq, 3jap, and 4v8z. Abbreviations: 30S-I, 30S initiation complex; 70S-E, elongation-competent 70S complex; 70S-I, 70S initiation complex; cryo-EM, cryo–electron microscopy; CTD, C-terminal domain; eIF, eukaryotic initiation factor; IF, initiation factor; NTD, N-terminal domain; rRNA, ribosomal RNA; tRNA, transfer RNA.

IF1 binds the 30S subunit A site and bridges IF2 and IF3 (**Figure 2*a***) (29–31). The GTPase IF2 recognizes the formyl-methionyl moiety of initiator tRNA (32) and coordinates the binding of the 50S subunit to form the 70S initiation complex (**Figure 2*a***). GTP hydrolysis by the sarcin-ricin loop (SRL) of the large subunit allows dissociation of IF2 and formation of the

elongation-competent 70S complex (70S-E), in which the fMet moiety is bound in the peptidyl transferase center (PTC), and the mRNA exposes the first elongation codon in the A site. IF3 plays a central role in initiation fidelity by discriminating against elongator tRNAs (33, 34). The dynamic IF3 (35) has evaded high-resolution structural characterization on the ribosome until recently (11). The N-terminal and C-terminal halves of IF3 align with the E and P sites, respectively, along the mRNA path. This destabilizes tRNA binding to the small subunit and, together with IF1, precludes premature subunit joining (36, 37).

How does the ribosome cooperate with initiation factors to select the initiator tRNA and to effectively discriminate against elongator tRNAs? Complementarity of the initiator tRNA anticodon to the start codon must be a key determinant of this discrimination. However, the differences in the thermodynamic stabilities of the cognate and mismatched base pairs are too small (38) to account for stringent discrimination of $>10^3$ fold (28). Rather, the ribosome and initiation factors rely on thermal fluctuations and meta-stability of the three-base-pair codon–anticodon helix to shift the equilibrium toward dissociation of mismatched tRNA or stabilization of cognate initiator tRNA (39). Cryo-EM ensembles of initiation structures suggest how the ribosome might accomplish this (11).

In the absence of fMet-RNA^{fMet}, the C-terminal domain (CTD) of IF3 shields the AUG codon in the P site and interacts with IF1, which blocks the A site (see the left side of **Figure 2*c***). The 30S subunit samples open and closed states, whereby the head tilts away from or toward the body, stochastically widening the mRNA tunnel by more than 10 Å (**Figure 2*a***). Binding of tRNA next to the AUG codon on the open 30S initiation complex (30S-I) requires a small shift of IF3 (see the middle of **Figure 2*c***). Three G–C pairs in the anticodon stem of tRNA^{fMet} are important for selecting and stabilizing the tRNA via interactions with G1338 and A1339 at the head of the 30S subunit (11, 40, 41). Further stabilization of tRNA coincides with the 30S subunit head tilt, which moves the head closer to the body than in the open state, thus latching the subunit. Latching of 30S-I (closed) requires dissociation of the IF3 CTD from the AUG codon and from IF1 (see the right side of **Figure 2*c***). Thus, the IF3 CTD works as a switch that prevents stable binding of tRNA unless a cognate Watson–Crick codon–anticodon helix is formed in the closed 30S state (**Figure 2*a***).

In the latched 30S-I (closed) complex, the ∼10-Å head tilt (at G1338) shifts the tRNA, moving the CCA-fMet end by ∼25 Å toward the body (**Figure 2*a***). In this position, tRNA^{fMet} interacts with IF2 bound at the 30S body (**Figure 2*a***), which triggers subunit joining. Formation of the 70S complex involves intersubunit dynamics that resemble those of translocation. Single-molecule (sm)FRET (42) and time-resolved cryo-EM (43) reveal that subunit joining with IF2 (to form 70S-I) involves partial head swivel and partial subunit rotation (∼4°). Upon IF2 dissociation, the ribosome adopts a nonrotated 70S-E conformation ready to bind the first elongator tRNA (**Figure 2*a***). Curiously, an earlier cryo-EM study captured a small population of fully rotated 70S•fMet-tRNA^{fMet} ribosomes with IF2 and the nonhydrolyzable GTP analog, GDPNP (44). This structure was proposed as an on-pathway intermediate of subunit joining. However, this fully rotated structure was not identified in the solution smFRET or time-resolved cryo-EM studies of GTP-catalyzed subunit joining, so the possible role of this structural state remains to be shown. Nevertheless, the specificity of IF2 for the initiator tRNA further contributes to initiation fidelity (32, 45), so the combination of all three initiation factors achieves the highest initiation efficiency and accuracy (28, 46, 47). In summary, recent studies visualized how initiation factors rectify the inherent 30S and 70S dynamics to bias initiation toward formation of the 70S complex with initiator tRNA. Restricting the conformational dynamics of the 30S subunit (e.g., with the antibiotic streptomycin) decreases initiation fidelity (46), in keeping with the essential role of ribosome rearrangements.

Several questions concerning the mechanism of initiation remain to be addressed. First, to delineate the roles of 30S rearrangements and IF3 in tRNA discrimination, structures of cognate initiation complexes need to be compared with those formed with near-cognate tRNAs. Biochemical studies showed that IF3 uniformly destabilizes binding of tRNAs to the 30S subunit, including initiator tRNA. Comparison of initiation complexes with different tRNAs is needed to visualize detailed structural differences that enable the ribosome to discriminate against near-cognate tRNAs. Second, current structural data do not distinguish whether initiation follows one or more pathways (**Figure 2*a***). For example, the capture of a closed 30S•IF3•fMet-tRNA^{fMet} complex without IF1 (**Figure 2*a***) suggests at least two scenarios: (*a*) IF1 can bind or dissociate at initial stages of tRNA recognition and thus contribute to tRNA discrimination or (*b*) IF1 binds 30S-I at a later stage to stabilize IF2 (48). Alternatively, parallel pathways of initiation that allow different orders of IF binding (11) would be consistent with differential regulation of translation on distinct mRNAs and under different cellular conditions. This idea remains to be reconciled with biochemical data suggesting a preferred pathway (48). Nevertheless, the existence of parallel pathways is an attractive hypothesis for translation and other regulated cellular processes that depend on multiple factors. For example, ribosomal subunit biosynthesis—when the newly made rRNA transcript is chaperoned by ribosomal proteins—proceeds via different orders of protein binding rather than being an orderly assembly line–like process (49).

Eukaryotic initiation has diverged considerably from bacterial initiation. It involves dozens of polypeptides forming initiation factors and interacting in complex ways to regulate translation from 5′-m^{7}G-capped mRNAs (reviewed in 50, 51). Yet, recent structural studies reveal mechanistic similarities, highlighting how the dynamics of the conserved small-subunit core determines the formation of the 80S initiation complex. Despite the absence of sequence homology, the functions of bacterial IF1 and the C- and N-terminal domains of IF3 are similar to those of the eukaryotic factors eIF1A, eIF1, and eIF2α, respectively (**Figure 2*d***) (52, 53). The eukaryotic 40S samples open and closed conformations, resulting in eIF1 dissociation upon tRNA recognition (54, 55), emphasizing the conserved mechanistic principles of initiation accuracy. Furthermore, the eukaryotic GTPase eIF5B recognizes the aminoacyl moiety of initiator tRNA and facilitates subunit joining, resembling bacterial IF2 (**Figure 2*d***) (56, 57). These similarities, along with the increased complexity of eukaryotic initiation, are consistent with the idea that eukaryotic initiation can proceed via multiple pathways, in keeping with the complex regulation of eukaryotic translation of different mRNAs.

3. ELONGATION

3.1. mRNA Decoding and tRNA Proofreading

Translation elongation involves a periodic repetition of three steps, as the ribosome moves along sense codons until it reaches the stop codon (**Figures 3** and **4**). First, the ribosome recognizes an aa-tRNA cognate to the A-site codon and rejects noncognate aa-tRNAs (decoding) (**Figure 3*a–b***). Second, the ribosome catalyzes formation of a peptide bond between the incoming cognate aa-tRNA and the P-site peptidyl-tRNA, resulting in peptidyl-tRNA in the A site and deacyl-tRNA in the P site (peptidyl transfer) (**Figure 3*i*,*j***). Third, the A-site and P-site tRNAs translocate, along with the mRNA, to the P and E sites, respectively, to allow the next round of elongation (translocation) (**Figure 4**). These steps have been extensively discussed in reviews (16, 58–64), so the following discussion focuses on the recent structural studies that visualize the roles of ribosome dynamics and elongation factors EF-Tu and EF-G in maintaining elongation accuracy.

The high accuracy of decoding, with only 10^{-3}–10^{-5} errors per codon (65), is essential for all life. It is achieved through the two-step selection of cognate tRNAs involving initial decoding and

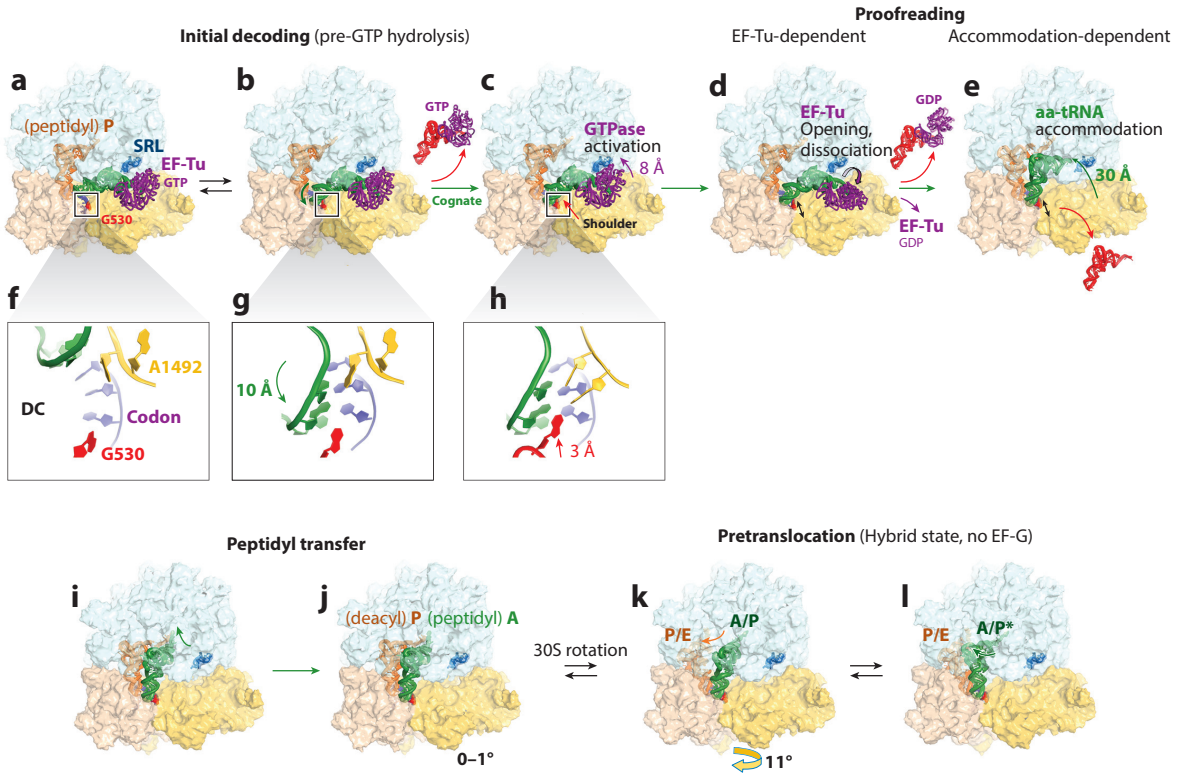

Figure 3

Ribosome, EF-Tu, and tRNA dynamics during mRNA decoding and tRNA proofreading, visualized by ensemble and time-resolved cryo-EM. (*a*) Binding of the aa-tRNA•EF-Tu•GTP ternary complex to the small subunit. (*b*) Codon recognition upon tRNA ASL tilting to base-pair with the mRNA codon. (*c*) A shift in G530 (*red*) and the 30S shoulder brings EF-Tu toward the SRL (*blue*), resulting in EF-Tu GTPase activation (80). (*d*) Movement of the GTPase domain of EF-Tu, resulting in EF-Tu rearrangement and dissociation. The 30S subunit continues to sample the open and closed conformations (82). (*e*) Following EF-Tu dissociation, cognate tRNA (*green*) is stably held by the 30S (closed) and accommodated into the 50S A site, while near-cognate tRNA continues to sample open 30S conformations and is prone to dissociation via proofreading. (*f–h*) Conformation of the decoding center during recognition of the tRNA anticodon (location approximately shown within the square in panel *b*). G530 (*red*) at the shoulder of the open 30S subunit (*f*) transiently stabilizes the codon–anticodon helix (*g*) then moves toward A1492 (*yellow*), resulting in 30S domain closure and tRNA locking (*h*). (*i–j*) Insertion of the aminoacyl-CCA moiety into the peptidyl-transferase center leads to elongation of the polypeptide and is accompanied by small 30S subunit rotation. (*k–l*) Large-scale 30S rotation relative to the 50S subunit coincides with tRNA movement on the 50S subunit and preparation for translocation: A/P for peptidyl-tRNA and P/E for deacyl-tRNA. The elbow of A/P tRNA can spontaneously move toward the P site, yielding A/P* tRNA, a substrate for EF-G binding to initiate translocation (panel *l*). The degrees of intersubunit rotation were measured relative to the previously published nonrotated posttranslocation 70S structure VII (97). Abbreviations: aa-tRNA, aminoacyl-tRNA; ASL, anticodon stem loop; cryo-EM, cryogenic electron microscopy; DC, decoding center; EF, elongation factor; SRL, sarcin-ricin loop.

kinetic proofreading (66, 67). The aa-tRNAs are delivered to the ribosome as part of the ternary complex with the universally conserved GTPase EF-Tu (eEF1A in eukaryotes) and GTP. When a cognate tRNA is successfully recognized, GTP hydrolysis releases EF-Tu. This irreversible reaction separates the biochemical steps of initial selection and proofreading, the latter allowing an incorrectly decoded near-cognate tRNA to be rejected prior to peptide bond formation.

Recent cryo-EM studies, supported by an extensive body of biochemical (e.g., 68–71), biophysical (e.g., 72–75), crystallographic (e.g., 12–14, 76), and computational (e.g., 77–79) studies, have

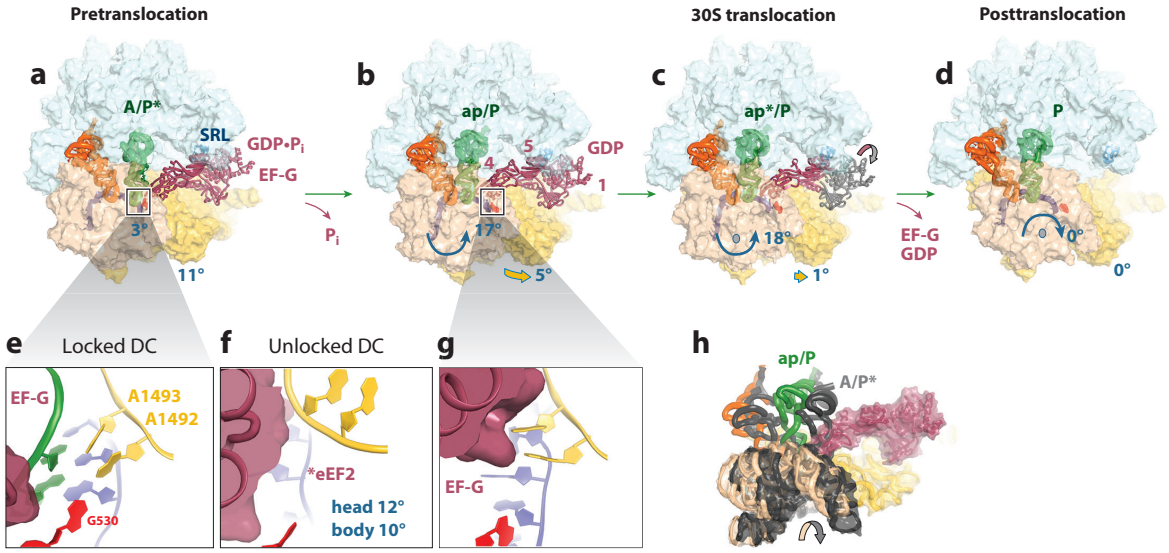

Figure 4

Cryo-EM structures of 70S translocation complexes visualized by ensemble and time-resolved cryo-EM with EF-G and GTP. The degrees of rotation are labeled for the small subunit body (*bold*) and head (*italics*). (*a*) Pretranslocation 70S ribosome with the fully rotated 30S bound with EF-G prior to P_i release (97). (*b*) 70S ribosome with extensive head swivel and intermediate body rotation, bound with EF-G with GDP (post P_i release) and chimeric tRNAs shifted by ∼20 Å relative to the A/P* tRNA in panel *a* (97). The GTPase (1) and translocase domains (4 and 5) of EF-G are labeled. (*c*) 70S ribosome with extensive head swivel and low body rotation, with ap*/P tRNA shifted by ∼4 Å relative to the ap/P tRNA in panel *b*. The GTPase superdomain of EF-G (*gray*) was not resolved in cryo-EM maps, consistent with dissociation from the SRL. (*d*) Posttranslocation nonrotated ribosome with tRNAs in the P and E sites. (*e*) The pretranslocation decoding center is locked by interactions between G530 and A1492–A1493, similar to the decoding structures shown in **Figure 3** (pretranslocation structure from panel *a* is shown). (*f*) Eukaryotic 80S•IRES•eEF2 structure (101) illustrates an early step of elongation factor entry into the A site, coupled with separation of the decoding center nucleotides (unlocking). (*g*) Position of EF-G in the A site in a late translocation state shown in panel *b*. (*h*) Superposition of pretranslocation (*gray*) and nearly posttranslocated (colored as in panel *b*) complexes, showing that EF-G would create steric hindrance for tRNA during reverse head swivel (shown by arrow). Superposition was performed by structural alignment of the 16S rRNA body domains (i.e., excluding head nucleotides 930–1,385). The degrees of intersubunit rotation were measured relative to the previously published nonrotated posttranslocation 70S structure VII (96). Abbreviations: cryo-EM, cryogenic electron microscopy; DC, decoding center; eEF, eukaryotic elongation factor; EF-G, elongation factor G; IRES, internal ribosome entry site; SRL, sarcin-ricin loop.

visualized how decoding is driven by 30S dynamics. Both the initial selection and proofreading steps were recently resolved in structural ensembles formed with EF-Tu prior to GTP hydrolysis (80, 81) and by uninhibited, time-resolved reactions with GTP and authentic aa-tRNAs (82). These structural ensembles reveal that initial selection and proofreading rely on the same 30S rearrangements. As part of the ternary complex, EF-Tu lands on the 30S subunit shoulder, presenting the tRNA anticodon at a ∼15-Å distance from the A-site codon (**Figure 3*a*,*f***). This initial mode of binding prevents GTP hydrolysis because EF-Tu's GTPase active site is ∼10 Å away from the 50S GTPase-activating SRL. The 30S subunit adopts a domain-open conformation in the absence of base-pairing between the codon and anticodon. Stochastic tRNA dynamics kink the ASL, bringing the anticodon toward the codon and allowing the formation of a codon–anticodon helix. A Watson–Crick helix is stabilized by hydrogen bonds with universally conserved 16S nucleotide G530 at the tip of the shoulder domain of 30S (**Figure 3*g***). The codon–anticodon RNA helix is further stabilized by transient interactions with decoding center nucleotides A1492–A1493 from the 30S body (**Figure 3*g***). In the presence of a cognate codon–anticodon helix, G530 and

the shoulder domain move ~3–5 Å closer to A1492–A1493, locking the tRNA in the decoding center of a domain-closed 30S subunit (**Figure 3*b***). Thus, transient positioning of G530 next to A1492, in the presence of a cognate codon–anticodon helix (**Figure 3*g***), shifts the equilibrium toward a domain-closed 30S (**Figure 3*b***). This motion brings the shoulder-bound EF-Tu toward the SRL, activating the EF-Tu GTPase domain.

Cryo-EM studies that compare decoding with cognate and near-cognate tRNAs revealed different interactions and populations of particles in structural ensembles. With cognate tRNA, the largest population of structures features G530 fully engaged in the decoding center of a domain-closed 30S. By contrast, near-cognate tRNA (with mismatches in the first or second positions) (80, 81) shifts the population toward domain-open 30S with G530 disengaged from the distorted near-cognate codon–anticodon helix. Thus, near-cognate tRNAs shift the equilibrium toward the domain-open 30S, preventing GTP hydrolysis and favoring ternary complex dissociation. Cognate tRNAs shift the equilibrium toward the domain-closed 30S, favoring EF-Tu GTPase activation.

Time-resolved cryo-EM visualized EF-Tu dissociation after GTP hydrolysis, consistent with two tRNA proofreading steps: EF-Tu-dependent and accommodation-dependent (82). In the domain-closed 30S, EF-Tu's GTPase center docks at the SRL, resulting in GTP hydrolysis (82, 83). Upon inorganic phosphate (P_i) release, the GTPase domain dissociates from the SRL, forming extended EF-Tu conformations (82) that resemble those in crystal structures of isolated EF-Tu•GDP (76). In the presence of EF-Tu•GDP, the shoulder of 30S continues to sample open and closed states, as the tRNA remains kinked to retain codon–anticodon interactions. The dynamics of the 30S subunit therefore suggests the possibility of tRNA dissociation with EF-Tu•GDP in a step proposed by biochemical studies to represent EF-Tu-dependent proofreading (**Figure 3*d***) (70). Following EF-Tu release, the cognate tRNA relaxes and accommodates into the A site of the large subunit, traversing ~80 Å from its initial EF-Tu-bound state (**Figure 3*e*,*f***). A slight rotation of the small subunit (~2.5°) likely allows the accommodating tRNA to bypass elements that protrude from the large subunit [e.g., H89, as identified in molecular dynamics simulations (78, 84)]. Remarkably, cryo-EM classifications found that during accommodation, cognate tRNA is stably bound (locked) in ribosomes with a closed 30S subunit, suggesting that the ribosome has committed to accept the cognate tRNA. By contrast, ribosomes with near-cognate tRNA continue to sample the open 30S subunit with disengaged G530. The instability of interactions between near-cognate tRNA and 30S during accommodation likely favors dissociation, representing accommodation-dependent proofreading (**Figure 3*e***). Thus, the same intrasubunit dynamics govern the initial tRNA selection and proofreading stages, accounting for high decoding accuracy.

3.2. Translocation of tRNA and mRNA

Accommodation of tRNA into the ribosomal A site results in peptidyl transfer from the P-to A-site tRNA. To prepare the ribosome for accepting the next tRNA, GTPase elongation factor (EF-G in bacteria and eEF-2 in eukaryotes) translocates the mRNA with deacyl-tRNA and peptidyl-tRNA (**Figure 3*i*,*j***) (for reviews, see 60–64). It is critical to maintain the open reading frame during translocation, when frameshifting may occur and result in a defective protein product (85, 86). Structural visualization of the fast GTP-catalyzed translocation has long remained a challenge. Numerous structural studies have captured EF-G with two tRNAs in the presence of EF-G mutations (87, 88), antibiotics (89–94), or nonhydrolyzable GTP analogs (95), but concerns have been raised that such approaches may capture off-pathway structures (96). A recent time-resolved cryo-EM study visualized translocation on the 70S ribosome by EF-G and GTP without inhibitors (97). Structures of pretranslocation and posttranslocation states along

with three EF-G-bound intermediates yielded a dynamic view of the translocation trajectory, supported by an extensive array of structural, biochemical, and FRET studies.

After peptidyl transfer, the two tRNAs spontaneously sample the hybrid A/P and P/E states (9, 98), coupled with a 10–11° rotation of the small subunit (**Figure 3*k***) (5, 99, 100). During these transitions, the elbow of the peptidyl-tRNA can shift ∼20 Å closer to the P site, adopting an A/P* state (**Figure 3*l***). EF-G•GTP binds to the rotated ribosome, placing the protein's translocase domain 4 near the A/P* tRNA, while EF-G domain 5 is anchored at the L11 stalk of the large subunit (**Figure 4*a***). During spontaneous reverse rotation of the 30S subunit (i.e., toward a nonrotated state), domain 4 sterically blocks peptidyl-tRNA. As a result, the tRNA and mRNA shift toward the P site on the small subunit, proceeding via intermediate stages of translocation (**Figure 4*b–d***) in which the head swivels toward the large subunit by ∼18° (97). The following discussion describes in more detail how EF-G and GTP catalyze translocation during reverse subunit rotation.

The initial binding of EF-G to the rotated ribosome (11.6° body rotation) places the tip of domain 4 (loop 1) next to G530, which, together with A1492 and A1493, stabilizes the peptidyl-tRNA in the A site (**Figure 4*e***) (97). To initiate translocation, EF-G must unlock the decoding center. A recent cryo-EM study captured EF-G with translocation inhibitor spectinomycin and a slightly translocated tRNA–mRNA helix (93). In a marginally less rotated ribosome•spectinomycin conformation (10.9° body rotation), loop 1 of EF-G is shifted toward A1493, and the codon–anticodon helix is disengaged from G530. This intermediate resembles a yeast 80S translocation structure captured earlier with tRNA-like internal ribosome entry site (IRES) mRNA and eEF-2 stalled by sordarin (**Figure 4*f***) (101). Although spectinomycin and sordarin could have perturbed the ribosome/elongation factor structures in these studies, their binding to different sites (the 30S and eEF2, respectively) yielded similar ribosome conformations. This suggests that the structures with disengaged G530 (G577 in yeast) likely mimic a conserved early intermediate of translocation.

Further reverse rotation of the 30S body (5°) shifts domain 4 deeper into the A site (**Figure 4*g***), concurrent with a ∼20-Å movement of peptidyl-tRNA into the P site and deacyl-tRNA into the E site of the 30S body, resulting in the ap/P and pe/E chimeric states, which could also be visualized in the presence of fusidic acid or nonhydrolyzable GTP analogs (91, 95). EF-G loops 1 and 2 shift closer to peptidyl-tRNA and mRNA, extending EF-G contact with the codon–anticodon helix. The 30S head rotates in the direction of tRNA translocation by ∼17° while keeping contact with the tRNAs and mRNA. Concurrent movement of EF-G and the 30S head during translocation are likely important for preservation of the open reading frame and prevention of frameshifting. Indeed, recent cryo-EM and FRET studies showed that frameshift-prone mRNAs and near-cognate tRNA can experience frameshifting during head swiveling in the course of EF-G-catalyzed translocation (86, 95). A crystal structure further corroborates the critical role of EF-G, demonstrating that without EF-G, the head-swiveled ribosome with a cognate tRNA fails to preserve Watson–Crick pairing of the codon–anticodon helix in the ap/P state (102).

The final EF-G bound state features a nearly nonrotated 30S body (1°) with the most swiveled head (18°) and tRNAs translocated further by ∼4 Å, yielding the ap*/P peptidyl-tRNA (**Figure 4*c***) (97). While the translocase domain of EF-G remains in the 30S A site, its GTPase superdomain (domains 1–2) has detached from the ribosome, suggesting an EF-G dissociation stage. Indeed, a similarly rotated ribosome state without EF-G has been detected in the same cryo-EM data set with translocation intermediates, consistent with EF-G dissociation from a head-swiveled ribosome. Reverse swivel of the 30S head restores the ribosomal A and P sites, preparing the ribosome for the next decoding event (**Figure 4*d***).

Recent advances in biochemical approaches and time-resolved cryo-EM have clarified the long-debated role of GTP in translocation. Since nonhydrolyzable GTP analogs and catalytically

dead EF-G mutants accelerate translocation by more than three orders of magnitude, similar to GTP (87, 103, 104), the hydrolysis of GTP does not substantially contribute to tRNA movement. Instead, GTP hydrolysis enables EF-G dissociation, yielding a functional posttranslocation ribosome with a vacant A site. Cryo-EM structures revealed that GTP or GTP analogs facilitate EF-G binding to the pretranslocation ribosome by enabling structural complementarity of the EF-G GTPase center to the SRL and rotated 30S subunit (94, 97). The GTPase domain of EF-G coordinates GTP via ordered switch loops, one of which (sw-1) bridges the SRL of the 50S subunit and the platform of the 30S subunit. Docking of EF-G at the SRL results in rapid GTP hydrolysis (105). The phosphate, however, remains in the catalytic pocket due to stabilization of the switch loop by the rotated 30S subunit. Reverse rotation separates the 30S from sw-1, resulting in phosphate dissociation, consistent with the kinetic coupling of translocation with phosphate release. Movement of EF-G into the 30S A site coincides with dissociation of the GTPase domain from the SRL (**Figure 4*c***), ultimately resulting in EF-G release and formation of the nonrotated posttranslocation ribosome. By contrast, the inability to hydrolyze GTP in studies with GTP analogs and catalytically inactive EF-G mutants yields EF-G attached to nonrotated posttranslocation ribosomes (87, 95). The inability of EF-G to dissociate modestly slows the reverse 30S rotation (8), consistent with a modest—twofold to 50-fold—decrease in translocation rate compared with GTP-catalyzed translocation (104, 106, 107). Thus, GTP hydrolysis and release of the phosphate allow EF-G dissociation, while EF-G catalyzes translocation by converting spontaneous ribosome fluctuations into tRNA translocation.

Recent cryo-EM studies emphasize the structural similarity of elongation in bacteria and eukaryotes, implicating a similar mechanism of elongation accuracy in eukaryotes. High-resolution 80S decoding complexes (108) and lower-resolution dynamics of eEF1A and the 40S subunit in decoding complexes (18) have been reported, although the detailed dynamics of codon recognition and proofreading remain to be visualized. A high-resolution understanding of eukaryotic translocation is also emerging (109), highlighting similarities between bacterial and eukaryotic translocases and small-subunit dynamics.

4. TERMINATION

Translation terminates when a stop codon arrives at the A site. Unlike sense codons, stop codons are recognized by proteins called release factors (RFs). RF1 and RF2 in bacteria terminate translation on the UAA/UAG and UAA/UGA stop codons, respectively. These bifunctional enzymes recognize the stop codon on the 30S subunit and catalyze hydrolysis of the peptidyl-tRNA ester linkage in the PTC, thus releasing a newly made protein from the ribosome. Biochemical, cryo-EM, and high-resolution crystallographic studies have revealed that RFs bind in the ribosomal A site and span the decoding center and the peptidyl-transferase center. The codon-recognition superdomain interacts with all three nucleotides of the stop codon on the 30S subunit. The catalytic domain crowned with the universally conserved GGQ motif is placed in the PTC. Here, the backbone NH group of the glutamine catalyzes the nucleophilic attack of a water molecule on the peptidyl-tRNA's ester linkage, resulting in peptide dissociation from the ribosome. The catalytic and codon-recognition domains are bridged by a switch loop, whose binding to the decoding center was proposed to be important for termination accuracy. The detailed mechanisms of stop-codon recognition and peptidyl-tRNA hydrolysis have been extensively reviewed (110, 111).

Two long-standing questions, however, remained unresolved until recent structural studies of RF and ribosome dynamics: (*a*) how is the RF activated by the stop codon? (*b*) how does the RF dissociate after termination? The strict coordination between codon recognition and

peptidyl-tRNA hydrolysis was proposed to be achieved via a large conformational change of the RF as it binds the A site. Keeping the GGQ away from the PTC during initial sampling of the A-site codon would allow the RF to dissociate without peptide release on a sense codon and thus prevent premature termination. Compact RFs were initially visualized in crystallographic structures of isolated RFs (112, 113) and in the studies of alternative ribosome-rescue factor ArfA, which acts with RF2 to recycle ribosomes stalled on a truncated mRNA, i.e., without a stop codon (114, 115). More recently, a hyperaccurate mutant of RF1 was crystallized with the PTC-binding antibiotic blasticidin S, which decouples codon recognition from insertion of the catalytic domain into the PTC (116) and suggests the presence of compact RF on the ribosome. Yet, capturing the canonical termination complex with a compact RF without inhibitors remained a challenge due to the fast rate of the conformational rearrangement (117, 118). After hydrolyzing the ester linkage of peptidyl-tRNA, the RF must dissociate from the A site to allow ribosomal subunit and deacyl-tRNA dissociation and recycling. Translational GTPase RF3, present in many bacteria, was shown to mediate RF1 release; however, RF2 can dissociate spontaneously (119). The function of RF3 is not essential for cell viability, indicating that both RFs can dissociate without RF3 (120, 121). One clue to the mechanism of RF dissociation is that RF3 stabilizes a rotated ribosome conformation (122, 123), arguing that intersubunit rotation is necessary for RF dissociation.

Recent cryo-EM studies address both questions and, together with previous studies, allow a structural reconstruction of the mechanism of termination. Time-resolved cryo-EM proved necessary to visualize the elusive rearrangements of RFs—from compact to extended (active) conformations—that couple codon recognition with peptidyl-tRNA hydrolysis on a time scale of tens of milliseconds (**Figure 5*a*,*b*,*f*,*g***) (118). RFs decode stop codons on the nonrotated ribosome (both head and body rotation are less than 1°). The inactive compact RF interacts with the stop codon with the catalytic domain ∼50 Å away from the PTC (**Figure 5*f*,*i***). The decoding center nucleotides are arranged to stabilize the mRNA (G530) (**Figure 5*i*,*j***) and the switch loop of RF (A1492, A1493) (**Figure 5*g*,*b***). To insert the catalytic domain into the PTC (**Figure 5*b***), the codon-recognition domain moves ∼3 Å to settle deeper in the decoding center (**Figure 5*j***). The tip of the switch loop (Trp319 in *E. coli* RF2) moves by 20 Å to interact with A1492 in the decoding center (**Figure 5*g***), consistent with the proposed essential role of the switch loop in termination (124). How RFs are rejected upon binding to a sense codon (**Figure 5*a*,*b***), however, remains to be determined, and this question requires studies that compare transient binding of RF to stop codons and sense codons.

A recent cryo-EM study of 70S•RF2 complexes uncovered a novel conformation of the catalytic domain of RF2, implicating a local conformational change in peptide release from the ribosome (125). In the canonical catalytic complexes, the loop containing the GGQ motif forms a short α-helix, which places the catalytic glutamine backbone group next to the ribose of the terminal P-tRNA residue A76 (**Figure 5*b***), the leaving group of the deacyl-tRNA product. Upon dissociation of the CCA^{76} tail from the PTC, however, the loop rearranges into a long β-hairpin, which extends into the peptide tunnel, as if plugging it to bias the newly formed protein to dissociate toward the 50S solvent surface (see the right side of **Figure 5*b***). This rearrangement underscores the flexibility of the GGQ motif and its possible function in nascent-protein dissociation from the ribosome.

Upon peptide release, the deacylated tRNA can dissociate from the PTC (**Figure 5*b***), allowing rotation of the small subunit (**Figure 5*b–d***). Consistent with FRET studies (119), recent cryo-EM studies reveal that RF-bound ribosomes sample large-scale 30S rearrangements. RF1 was visualized in the presence of RF3 and the antibiotic Apidaecin 137, which stalls RF1 in the PTC (126). RF2 was captured without RF3 and inhibitors (125). Each study resolved structural ensembles showing that RFs can remain in the ribosomal A site, while the small subunit spontaneously

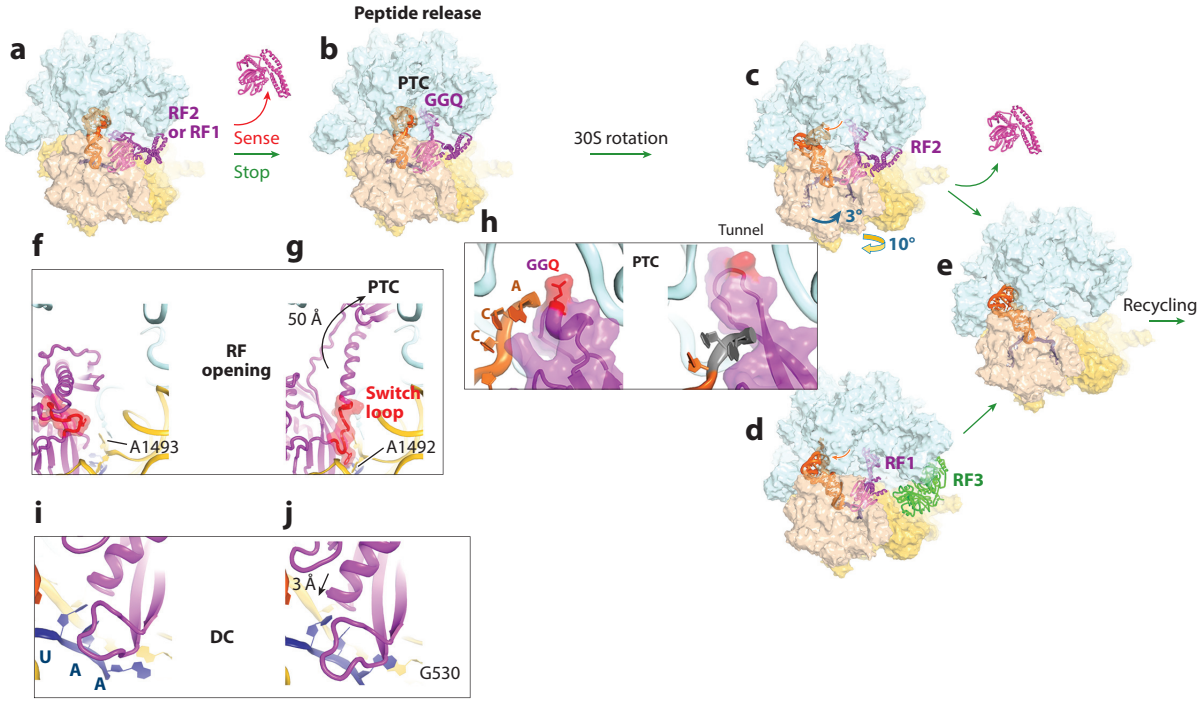

Figure 5

Release factor and ribosome rearrangements during termination. (*a–e*) Recent time-resolved and ensemble cryo-EM structures reveal the mechanism of peptide release by RF1 and RF2, from RF opening (118) to ribosome intersubunit rearrangements leading to RF dissociation (125, 126). (*f–g*, *i–j*) A close-up view of the DC and stop codon in the structures with the inactive compact and catalytic open RF2 (*magenta*) demonstrates how the catalytic domain and stop codon settle in the DC, leading to peptidyl-tRNA hydrolysis. (*h*) The catalytic GGQ motif adopts distinct conformations in the PTC, with the catalytically engaged α-helical (*left*; PDB ID: 4v67) and noncatalytic β-hairpin (*right*; PDB ID: 5u9f) plugging the peptide tunnel upon peptide release. The degrees of intersubunit rotation were measured relative to the previously published nonrotated posttranslocation 70S structure VII (97). Abbreviations: cryo-EM, cryogenic electron microscopy; DC, decoding center; PDB ID, Protein Data Bank identifier; PTC, peptidyl transferase center; RF, release factor.

adopts intermediate rotational states and the tRNA acceptor arm fluctuates between the P and E sites of the 50S subunit (**Figure 5*c*,*d***). Partial 30S head swivel (3° to 7° in the 70S•RF1•RF3 and 70S•RF2 structures) restructures the decoding center, disrupting interactions with the RF's codon-recognition superdomain. Both studies also observed a fully rotated 70S conformation with hybrid P/E tRNA but without an RF (**Figure 5*e***). Thus, completion of intersubunit rotation is likely coupled with RF dissociation. The remarkable similarity between RF1- and RF2-bound ribosomes indicates the use of similar mechanisms for RF recycling and for preparation of the ribosome for subunit splitting and tRNA dissociation by ribosome recycling factor (RRF) and EF-G. Indeed, time-resolved cryo-EM visualized recruitment of RRF and EF-G•GTP to rotated ribosomes and suggested that reverse 30S rotation acts to catalyze tRNA dislodging and subunit splitting (127). In the RF-bound posttermination states, the 30S rotation and head swivel occur similarly to those during late initiation steps, featuring the same pivot points and similarly aligned axes of rotation (**Figure 1*e***), highlighting the fact that RFs and initiation factors rely similarly on the inherent spontaneous ribosome dynamics.

Eukaryotic termination substantially differs from bacterial termination, yet they share the general principle of achieving termination fidelity via the opening of a RF. High-resolution cryo-EM

structures have revealed how eRF1 recognizes four mRNA nucleotides of the A site, highlighting the importance of a purine residue (i.e., G or A) following the canonical UAA, UGA, or UAG termination codons (128), consistent with biochemical, genomic, and cellular studies (129–131). Unlike bacterial RFs, eRF1 decodes the stop codons as a heterodimer with GTPase eRF3. The latter functionally mimics EF-Tu, so the eRF1•eRF3•GTP complex resembles the ternary complex during decoding. Cryo-EM structures revealed that eRF1 adopts a compact conformation in the presence of eRF3 and nonhydrolyzable GTP analogs (108, 132). Upon eRF3 dissociation, eRF1's catalytic domain extends to insert the GGQ motif into the PTC, so the chemical mechanism of peptidyl-tRNA hydrolysis is likely similar to that of bacterial RFs. The eukaryotic ATP-binding cassette protein ABCE1 then binds next to eRF1 (108, 133) to recycle the ribosome (134). Many dynamic steps, from eRF1 conformational rearrangements and eRF3 dissociation to ABCE1 binding and eRF1 dissociation, remain to be visualized. It is possible that, like the bacterial mechanisms, eukaryotic termination and recycling coopt 80S rearrangements, including intersubunit rotation, to facilitate posttermination recycling steps.

5. CONCLUDING REMARKS

5.1. Convergence of Mechanistic Insights from Cryo–Electron Microscopy and Other Methods

Rapid advances in cryo-EM technology have enabled the identification of many new structures. The convergence of insights from mutational, genetic, biochemical, and biophysical data has been essential for developing the mechanistic understanding of translation. Structure-based fluorescent techniques have been particularly complementary with structural techniques because they allowed the visualization and biophysical characterization of translation steps in solution, exploiting the structural positions of the reporter dyes. Perhaps the most notable example of convergence between cryo-EM and FRET has been the demonstration of large-scale intersubunit rotation, first by cryo-EM (2), then by bulk FRET in solution (122), and then with smFRET yielding the kinetics of intersubunit rotation and its coupling with tRNA and mRNA translocation (5). However, some cryo-EM structures that suggest mechanistic insights remain to be confirmed by FRET and vice versa. This gap could reflect the limitations of FRET studies (e.g., time resolution), differences in buffer conditions, off-pathway structures captured by cryo-EM, or other factors. Cryo-EM and FRET findings remain to be reconciled in all three steps of translation. In initiation, a fully rotated IF2-bound ribosome with GDPNP has been detected by cryo-EM, but only the semirotated 70S•IF2•tRNA state was reported by smFRET (42) and time-resolved cryo-EM with GTP (43). A fully rotated initiation-like complex with the initiator tRNA interacting with the L1 stalk, as in translocating P/E tRNAs, could be a short-lived intermediate of initiation that remains to be confirmed. Furthermore, capturing the complex interactions of all initiation factors during initiation remains a challenge for both techniques (11, 43) and is likely to be tackled by multi-dye FRET approaches (e.g., 135) and cryo-EM with deep classification (82) or other algorithms to deconvolute compositional and conformational heterogeneity (e.g., 136). In elongation, additional authentic states must exist with ribosome and EF-G rearrangements beyond the three translocation intermediates recently detected with EF-G and GTP (97). Future time-resolved cryo-EM studies will also visualize the details of mRNA frameshifting in both directions during elongation (+1 and −1). In addition, the correlation of posttermination ribosome rotation with RF release, proposed by cryo-EM studies, remains to be demonstrated by smFRET or other approaches.

The steps of translation are best characterized for bacterial translation, which has historically been the most widely studied translation system. Nevertheless, fast progress is being made in the cryo-EM characterization of archaeal (e.g., 137, 138), eukaryotic cytoplasmic (e.g., 139, 140), and

mitochondrial (e.g., 141–143) translation that will soon allow a complete visualization of translation steps in all kingdoms of life.

5.2. Ribosome Dynamics in Cellular Processes Beyond Translation

The ribosome is a key cellular sensor that interacts with numerous proteins or machineries beyond those directly involved in translation. Recent cryo-EM and biophysical studies revealed that inherent ribosome dynamics are remarkably similar among translation steps, underscoring the fact that distinct translation factors are used not to induce ribosome dynamics but to restrict (initiation factors and EF-Tu) or coopt (EF-G and RFs) spontaneous ribosome motions to achieve a high accuracy and efficiency of translation. The ribosome's interactions with many cellular macromolecules are also likely to involve similar dynamics to achieve their functional roles. High-resolution cryo-EM structures of large assemblies with RNA polymerase (reviewed in 144), mRNA-binding complexes (e.g., 145), diribosomes, and higher-order ribosome assemblies (146) have begun to uncover mechanisms that control transcription-translation coupling and mRNA quality control. They similarly implicate the dynamics of the small subunit, with distinct head tilts in the 30S complex with RNA polymerase (147) and 30S rotation in 70S•RNAP complexes and in the stalled ribosomes (146, 148). In future studies, in situ visualization of intraribosomal transitions and supramolecular ribosome complexes will be enabled by the rapid advances in cryogenic electron tomography (cryo-ET) and subtomogram averaging (149). Furthermore, structural features of individual macromolecules in the cellular environment will become identifiable with high-resolution approaches such as template matching that take advantage of databases of cryo-EM or X-ray structures (150).

DISCLOSURE STATEMENT

The authors are not aware of any affiliations, memberships, funding, or financial holdings that might be perceived as affecting the objectivity of this review.

ACKNOWLEDGMENTS

I thank Christine E. Carbone, Darryl Conte Jr., Dmitri N. Ermolenko, and Anna B. Loveland for discussions and comments on the manuscript. I apologize to those whose important work could not be discussed and cited due to space limitations. This work was funded by research grants from the Cystic Fibrosis Foundation (application #670773) and the National Institutes of Health (grant R35 GM127094).

LITERATURE CITED

1. Spirin AS. 1969. A model of the functioning ribosome: locking and unlocking of the ribosome subparticles. *Cold Spring Harb. Symp. Quant. Biol.* 34:197–207
2. Frank J, Agrawal RK. 2000. A ratchet-like inter-subunit reorganization of the ribosome during translocation. *Nature* 406:318–22
3. Ratje AH, Loerke J, Mikolajka A, Brunner M, Hildebrand PW, et al. 2010. Head swivel on the ribosome facilitates translocation by means of intra-subunit tRNA hybrid sites. *Nature* 468:713–16
4. Schuwirth BS, Borovinskaya MA, Hau CW, Zhang W, Vila-Sanjurjo A, et al. 2005. Structures of the bacterial ribosome at 3.5 Å resolution. *Science* 310:827–34
5. Cornish PV, Ermolenko DN, Noller HF, Ha T. 2008. Spontaneous intersubunit rotation in single ribosomes. *Mol. Cell* 30:578–88
6. Wasserman MR, Alejo JL, Altman RB, Blanchard SC. 2016. Multiperspective smFRET reveals rate-determining late intermediates of ribosomal translocation. *Nat. Struct. Mol. Biol.* 23:333–41

7. Guo Z, Noller HF. 2012. Rotation of the head of the 30S ribosomal subunit during mRNA translocation. *PNAS* 109:20391–94
8. Ermolenko DN, Noller HF. 2011. mRNA translocation occurs during the second step of ribosomal intersubunit rotation. *Nat. Struct. Mol. Biol.* 18:457–62
9. Blanchard SC, Kim HD, Gonzalez RL Jr., Puglisi JD, Chu S. 2004. tRNA dynamics on the ribosome during translation. *PNAS* 101:12893–98
10. Jahagirdar D, Jha V, Basu K, Gomez-Blanco J, Vargas J, Ortega J. 2020. Alternative conformations and motions adopted by 30S ribosomal subunits visualized by cryo–electron microscopy. *RNA* 26:2017–30
11. Hussain T, Llácer JL, Wimberly BT, Kieft JS, Ramakrishnan V. 2016. Large-scale movements of IF3 and tRNA during bacterial translation initiation. *Cell* 167:133–44.e13
12. Ogle JM, Brodersen DE, Clemons WM Jr., Tarry MJ, Carter AP, Ramakrishnan V. 2001. Recognition of cognate transfer RNA by the 30S ribosomal subunit. *Science* 292:897–902
13. Ogle JM, Ramakrishnan V. 2005. Structural insights into translational fidelity. *Annu. Rev. Biochem.* 74:129–77
14. Demeshkina N, Jenner L, Westhof E, Yusupov M, Yusupova G. 2012. A new understanding of the decoding principle on the ribosome. *Nature* 484:256–59
15. Korostelev A, Ermolenko DN, Noller HF. 2008. Structural dynamics of the ribosome. *Curr. Opin. Chem. Biol.* 12:674–83
16. Frank J, Gonzalez RL Jr. 2010. Structure and dynamics of a processive Brownian motor: the translating ribosome. *Annu. Rev. Biochem.* 79:381–412
17. Blanchard SC. 2009. Single-molecule observations of ribosome function. *Curr. Opin. Struct. Biol.* 19:103–9
18. Behrmann E, Loerke J, Budkevich TV, Yamamoto K, Schmidt A, et al. 2015. Structural snapshots of actively translating human ribosomes. *Cell* 161:845–57
19. Ma J, Campbell A, Karlin S. 2002. Correlations between Shine-Dalgarno sequences and gene features such as predicted expression levels and operon structures. *J. Bacteriol.* 184:5733–45
20. O'Connor M, Gregory ST, Rajbhandary UL, Dahlberg AE. 2001. Altered discrimination of start codons and initiator tRNAs by mutant initiation factor 3. *RNA* 7:969–78
21. Gualerzi CO, Pon CL. 2015. Initiation of mRNA translation in bacteria: structural and dynamic aspects. *Cell Mol. Life Sci.* 72:4341–67
22. Milon P, Rodnina MV. 2012. Kinetic control of translation initiation in bacteria. *Crit. Rev. Biochem. Mol. Biol.* 47:334–48
23. Shine J, Dalgarno L. 1974. The 3′-terminal sequence of *Escherichia coli* 16S ribosomal RNA: complementarity to nonsense triplets and ribosome binding sites. *PNAS* 71:1342–46
24. Steitz JA, Jakes K. 1975. How ribosomes select initiator regions in mRNA: base pair formation between the 3′ terminus of 16S rRNA and the mRNA during initiation of protein synthesis in *Escherichia coli*. *PNAS* 72:4734–38
25. Kaminishi T, Wilson DN, Takemoto C, Harms JM, Kawazoe M, et al. 2007. A snapshot of the 30S ribosomal subunit capturing mRNA via the Shine-Dalgarno interaction. *Structure* 15:289–97
26. Korostelev A, Trakhanov S, Asahara H, Laurberg M, Lancaster L, Noller HF. 2007. Interactions and dynamics of the Shine–Dalgarno helix in the 70S ribosome. *PNAS* 104:16840–43
27. Ringquist S, Jones T, Snyder EE, Gibson T, Boni I, Gold L. 1995. High-affinity RNA ligands to *Escherichia coli* ribosomes and ribosomal protein S1: comparison of natural and unnatural binding sites. *Biochemistry* 34:3640–48
28. Antoun A, Pavlov MY, Lovmar M, Ehrenberg M. 2006. How initiation factors maximize the accuracy of tRNA selection in initiation of bacterial protein synthesis. *Mol. Cell* 23:183–93
29. Simonetti A, Marzi S, Myasnikov AG, Fabbretti A, Yusupov M, et al. 2008. Structure of the 30S translation initiation complex. *Nature* 455:416–20
30. Julian P, Milon P, Agirrezabala X, Lasso G, Gil D, et al. 2011. The cryo-EM structure of a complete 30S translation initiation complex from *Escherichia coli*. *PLOS Biol.* 9:e1001095
31. Carter AP, Clemons WM Jr., Brodersen DE, Morgan-Warren RJ, Hartsch T, et al. 2001. Crystal structure of an initiation factor bound to the 30S ribosomal subunit. *Science* 291:498–501

32. Wu XQ, RajBhandary UL. 1997. Effect of the amino acid attached to *Escherichia coli* initiator tRNA on its affinity for the initiation factor IF2 and on the IF2 dependence of its binding to the ribosome. *J. Biol. Chem.* 272:1891–95
33. Hartz D, Binkley J, Hollingsworth T, Gold L. 1990. Domains of initiator tRNA and initiation codon crucial for initiator tRNA selection by *Escherichia coli* IF3. *Genes Dev.* 4:1790–800
34. Petrelli D, LaTeana A, Garofalo C, Spurio R, Pon CL, Gualerzi CO. 2001. Translation initiation factor IF3: two domains, five functions, one mechanism? *EMBO J.* 20:4560–69
35. Elvekrog MM, Gonzalez RL Jr. 2013. Conformational selection of translation initiation factor 3 signals proper substrate selection. *Nat. Struct. Mol. Biol.* 20:628–33
36. Grunberg-Manago M, Dessen P, Pantaloni D, Godefroy-Colburn T, Wolfe AD, Dondon J. 1975. Light-scattering studies showing the effect of initiation factors on the reversible dissociation of *Escherichia coli* ribosomes. *J. Mol. Biol.* 94:461–78
37. Grigoriadou C, Marzi S, Pan D, Gualerzi CO, Cooperman BS. 2007. The translational fidelity function of IF3 during transition from the 30 S initiation complex to the 70 S initiation complex. *J. Mol. Biol.* 373:551–61
38. Freier SM, Kierzek R, Caruthers MH, Neilson T, Turner DH. 1986. Free energy contributions of G•U and other terminal mismatches to helix stability. *Biochemistry* 25:3209–13
39. Caban K, Gonzalez RL Jr. 2015. The emerging role of rectified thermal fluctuations in initiator aa-tRNA- and start codon selection during translation initiation. *Biochimie* 114:30–38
40. Korostelev A, Trakhanov S, Laurberg M, Noller HF. 2006. Crystal structure of a 70S ribosome-tRNA complex reveals functional interactions and rearrangements. *Cell* 126:1065–77
41. Lancaster L, Noller HF. 2005. Involvement of 16S rRNA nucleotides G1338 and A1339 in discrimination of initiator tRNA. *Mol. Cell* 20:623–32
42. Ling C, Ermolenko DN. 2015. Initiation factor 2 stabilizes the ribosome in a semirotated conformation. *PNAS* 112:15874–79
43. Kaledhonkar S, Fu Z, Caban K, Li W, Chen B, et al. 2019. Late steps in bacterial translation initiation visualized using time-resolved cryo-EM. *Nature* 570:400–4
44. Sprink T, Ramrath DJ, Yamamoto H, Yamamoto K, Loerke J, et al. 2016. Structures of ribosome-bound initiation factor 2 reveal the mechanism of subunit association. *Sci. Adv.* 2:e1501502
45. Roy B, Liu Q, Shoji S, Fredrick K. 2018. IF2 and unique features of initiator $tRNA^{fMet}$ help establish the translational reading frame. *RNA Biol.* 15:604–13
46. Milon P, Konevega AL, Gualerzi CO, Rodnina MV. 2008. Kinetic checkpoint at a late step in translation initiation. *Mol. Cell* 30:712–20
47. Wintermeyer W, Gualerzi C. 1983. Effect of *Escherichia coli* initiation factors on the kinetics of *N*-AcPhe-$tRNA^{Phe}$ binding to 30S ribosomal subunits. A fluorescence stopped-flow study. *Biochemistry* 22:690–94
48. Milon P, Maracci C, Filonava L, Gualerzi CO, Rodnina MV. 2012. Real-time assembly landscape of bacterial 30S translation initiation complex. *Nat. Struct. Mol. Biol.* 19:609–15
49. Davis JH, Tan YZ, Carragher B, Potter CS, Lyumkis D, Williamson JR. 2016. Modular assembly of the bacterial large ribosomal subunit. *Cell* 167:1610–22.e15
50. Hinnebusch AG, Lorsch JR. 2012. The mechanism of eukaryotic translation initiation: new insights and challenges. *Cold Spring Harb. Perspect. Biol.* 4:a011544
51. Jackson RJ, Hellen CU, Pestova TV. 2010. The mechanism of eukaryotic translation initiation and principles of its regulation. *Nat. Rev. Mol. Cell Biol.* 11:113–27
52. Aylett CH, Boehringer D, Erzberger JP, Schaefer T, Ban N. 2015. Structure of a yeast 40S–eIF1–eIF1A–eIF3–eIF3j initiation complex. *Nat. Struct. Mol. Biol.* 22:269–71
53. Simonetti A, Guca E, Bochler A, Kuhn L, Hashem Y. 2020. Structural insights into the mammalian late-stage initiation complexes. *Cell Rep.* 31:107497
54. Llacer JL, Hussain T, Marler L, Aitken CE, Thakur A, et al. 2015. Conformational differences between open and closed states of the eukaryotic translation initiation complex. *Mol. Cell* 59:399–412
55. Hussain T, Llacer JL, Fernandez IS, Munoz A, Martin-Marcos P, et al. 2014. Structural changes enable start codon recognition by the eukaryotic translation initiation complex. *Cell* 159:597–607
56. Wang J, Johnson AG, Lapointe CP, Choi J, Prabhakar A, et al. 2019. eIF5B gates the transition from translation initiation to elongation. *Nature* 573:605–8

57. Fernandez IS, Bai XC, Hussain T, Kelley AC, Lorsch JR, et al. 2013. Molecular architecture of a eukaryotic translational initiation complex. *Science* 342:1240585
58. Pavlov MY, Ehrenberg M. 2018. Substrate-induced formation of ribosomal decoding center for accurate and rapid genetic code translation. *Annu. Rev. Biophys.* 47:525–48
59. Rodnina MV, Fischer N, Maracci C, Stark H. 2017. Ribosome dynamics during decoding. *Philos. Trans. R. Soc. B* 372:20160182
60. Ling C, Ermolenko DN. 2016. Structural insights into ribosome translocation. *WIREs RNA* 7:620–36
61. Noller HF, Lancaster L, Zhou J, Mohan S. 2017. The ribosome moves: RNA mechanics and translocation. *Nat. Struct. Mol. Biol.* 24:1021–27
62. Voorhees RM, Ramakrishnan V. 2013. Structural basis of the translational elongation cycle. *Annu. Rev. Biochem.* 82:203–36
63. Prabhakar A, Puglisi EV, Puglisi JD. 2019. Single-molecule fluorescence applied to translation. *Cold Spring Harb. Perspect. Biol.* 11:a032714
64. Rodnina MV, Peske F, Peng BZ, Belardinelli R, Wintermeyer W. 2019. Converting GTP hydrolysis into motion: versatile translational elongation factor G. *Biol. Chem.* 401:131–42
65. Wohlgemuth I, Pohl C, Rodnina MV. 2010. Optimization of speed and accuracy of decoding in translation. *EMBO J.* 29:3701–9
66. Hopfield JJ. 1974. Kinetic proofreading: a new mechanism for reducing errors in biosynthetic processes requiring high specificity. *PNAS* 71:4135–39
67. Thompson RC, Stone PJ. 1977. Proofreading of the codon-anticodon interaction on ribosomes. *PNAS* 74:198–202
68. Pape T, Wintermeyer W, Rodnina M. 1999. Induced fit in initial selection and proofreading of aminoacyl-tRNA on the ribosome. *EMBO J.* 18:3800–7
69. Zhang J, Ieong KW, Johansson M, Ehrenberg M. 2015. Accuracy of initial codon selection by aminoacyl-tRNAs on the mRNA-programmed bacterial ribosome. *PNAS* 112:9602–7
70. Ieong KW, Uzun U, Selmer M, Ehrenberg M. 2016. Two proofreading steps amplify the accuracy of genetic code translation. *PNAS* 113:13744–49
71. Kothe U, Rodnina MV. 2006. Delayed release of inorganic phosphate from elongation factor Tu following GTP hydrolysis on the ribosome. *Biochemistry* 45:12767–74
72. Geggier P, Dave R, Feldman MB, Terry DS, Altman RB, et al. 2010. Conformational sampling of aminoacyl-tRNA during selection on the bacterial ribosome. *J. Mol. Biol.* 399:576–95
73. Blanchard SC, Gonzalez RL, Kim HD, Chu S, Puglisi JD. 2004. tRNA selection and kinetic proofreading in translation. *Nat. Struct. Mol. Biol.* 11:1008–14
74. Gonzalez RL Jr., Chu S, Puglisi JD. 2007. Thiostrepton inhibition of tRNA delivery to the ribosome. *RNA* 13:2091–97
75. Liu W, Chen C, Kavaliauskas D, Knudsen CR, Goldman YE, Cooperman BS. 2015. EF-Tu dynamics during pre-translocation complex formation: EF-Tu•GDP exits the ribosome via two different pathways. *Nucleic Acids Res.* 43:9519–28
76. Polekhina G, Thirup S, Kjeldgaard M, Nissen P, Lippmann C, Nyborg J. 1996. Helix unwinding in the effector region of elongation factor EF-Tu-GDP. *Structure* 4:1141–51
77. Noel JK, Whitford PC. 2016. How EF-Tu can contribute to efficient proofreading of aa-tRNA by the ribosome. *Nat. Commun.* 7:13314
78. Sanbonmatsu KY, Joseph S, Tung CS. 2005. Simulating movement of tRNA into the ribosome during decoding. *PNAS* 102:15854–59
79. Warias M, Grubmuller H, Bock LV. 2020. tRNA dissociation from EF-Tu after GTP hydrolysis: primary steps and antibiotic inhibition. *Biophys. J.* 118:151–61
80. Loveland AB, Demo G, Grigorieff N, Korostelev AA. 2017. Ensemble cryo-EM elucidates the mechanism of translation fidelity. *Nature* 546:113–17
81. Fislage M, Zhang J, Brown ZP, Mandava CS, Sanyal S, et al. 2018. Cryo-EM shows stages of initial codon selection on the ribosome by aa-tRNA in ternary complex with GTP and the GTPase-deficient EF-TuH84A. *Nucleic Acids Res.* 46:5861–74
82. Loveland AB, Demo G, Korostelev AA. 2020. Cryo-EM of elongating ribosome with EF-Tu•GTP elucidates tRNA proofreading. *Nature* 584:640–45

83. Voorhees RM, Schmeing TM, Kelley AC, Ramakrishnan V. 2010. The mechanism for activation of GTP hydrolysis on the ribosome. *Science* 330:835–38
84. Whitford PC, Geggier P, Altman RB, Blanchard SC, Onuchic JN, Sanbonmatsu KY. 2010. Accommodation of aminoacyl-tRNA into the ribosome involves reversible excursions along multiple pathways. *RNA* 16:1196–204
85. Choi J, O'Loughlin S, Atkins JF, Puglisi JD. 2020. The energy landscape of −1 ribosomal frameshifting. *Sci. Adv.* 6:eaax6969
86. Gamper H, Li H, Masuda I, Robkis DM, Christian T, et al. 2021. Insights into genome recoding from the mechanism of a classic +1-frameshifting tRNA. *Nat. Commun.* 12:328
87. Li W, Liu Z, Koripella RK, Langlois R, Sanyal S, Frank J. 2015. Activation of GTP hydrolysis in mRNA-tRNA translocation by elongation factor G. *Sci. Adv.* 1:1500169
88. Lin J, Gagnon MG, Bulkley D, Steitz TA. 2015. Conformational changes of elongation factor G on the ribosome during tRNA translocation. *Cell* 160:219–27
89. Brilot AF, Korostelev AA, Ermolenko DN, Grigorieff N. 2013. Structure of the ribosome with elongation factor G trapped in the pretranslocation state. *PNAS* 110:20994–99
90. Zhou J, Lancaster L, Donohue JP, Noller HF. 2013. Crystal structures of EF-G-ribosome complexes trapped in intermediate states of translocation. *Science* 340:1236086
91. Ramrath DJ, Lancaster L, Sprink T, Mielke T, Loerke J, et al. 2013. Visualization of two transfer RNAs trapped in transit during elongation factor G-mediated translocation. *PNAS* 110:20964–69
92. Gao YG, Selmer M, Dunham CM, Weixlbaumer A, Kelley AC, Ramakrishnan V. 2009. The structure of the ribosome with elongation factor G trapped in the posttranslocational state. *Science* 326:694–99
93. Rundlet EJ, Holm M, Schacherl M, Natchiar SK, Altman RB, et al. 2021. Structural basis of early translocation events on the ribosome. *Nature* 595:741–45
94. Petrychenko V, Peng B-Z, Schwarzer ACAP, Peske F, Rodnina MV, Fischer N. 2021. Structural mechanism of GTPase-powered ribosome-tRNA movement. *Nat. Commun.* 12:5933
95. Demo G, Gamper HB, Loveland AB, Masuda I, Carbone CE, et al. 2021. Structural basis for +1 ribosomal frameshifting during EF-G-catalyzed translocation. *Nat. Commun.* 12:4644
96. Holtkamp W, Cunha CE, Peske F, Konevega AL, Wintermeyer W, Rodnina MV. 2014. GTP hydrolysis by EF-G synchronizes tRNA movement on small and large ribosomal subunits. *EMBO J.* 33:1073–85
97. Carbone CE, Loveland AB, Gamper HB Jr., Hou YM, Demo G, Korostelev AA. 2021. Time-resolved cryo-EM visualizes ribosomal translocation with EF-G and GTP. *Nat. Commun.* 12:7236
98. Moazed D, Noller HF. 1989. Intermediate states in the movement of transfer RNA in the ribosome. *Nature* 342:142–48
99. Agirrezabala X, Lei J, Brunelle JL, Ortiz-Meoz RF, Green R, Frank J. 2008. Visualization of the hybrid state of tRNA binding promoted by spontaneous ratcheting of the ribosome. *Mol. Cell* 32:190–97
100. Fischer N, Konevega AL, Wintermeyer W, Rodnina MV, Stark H. 2010. Ribosome dynamics and tRNA movement by time-resolved electron cryomicroscopy. *Nature* 466:329–33
101. Abeyrathne PD, Koh CS, Grant T, Grigorieff N, Korostelev AA. 2016. Ensemble cryo-EM uncovers inchworm-like translocation of a viral IRES through the ribosome. *eLife* 5:e14874
102. Zhou J, Lancaster L, Donohue JP, Noller HF. 2019. Spontaneous ribosomal translocation of mRNA and tRNAs into a chimeric hybrid state. *PNAS* 116:7813–18
103. Gavrilova LP, Kostiashkina OE, Koteliansky VE, Rutkevitch NM, Spirin AS. 1976. Factor-free ("non-enzymic") and factor-dependent systems of translation of polyuridylic acid by *Escherichia coli* ribosomes. *J. Mol. Biol.* 101:537–52
104. Rodnina MV, Savelsbergh A, Katunin VI, Wintermeyer W. 1997. Hydrolysis of GTP by elongation factor G drives tRNA movement on the ribosome. *Nature* 385:37–41
105. Katunin VI, Savelsbergh A, Rodnina MV, Wintermeyer W. 2002. Coupling of GTP hydrolysis by elongation factor G to translocation and factor recycling on the ribosome. *Biochemistry* 41:12806–12
106. Chen J, Petrov A, Tsai A, O'Leary SE, Puglisi JD. 2013. Coordinated conformational and compositional dynamics drive ribosome translocation. *Nat. Struct. Mol. Biol.* 20:718–27
107. Salsi E, Farah E, Ermolenko DN. 2016. EF-G activation by phosphate analogs. *J. Mol. Biol.* 428:2248–58
108. Shao S, Murray J, Brown A, Taunton J, Ramakrishnan V, Hegde RS. 2016. Decoding mammalian ribosome-mRNA states by translational GTPase complexes. *Cell* 167:1229–40.e15

109. Flis J, Holm M, Rundlet EJ, Loerke J, Hilal T, et al. 2018. tRNA translocation by the eukaryotic 80S ribosome and the impact of GTP hydrolysis. *Cell Rep*. 25:2676–88.e7
110. Korostelev AA. 2011. Structural aspects of translation termination on the ribosome. *RNA* 17:1409–21
111. Rodnina MV. 2018. Translation in prokaryotes. *Cold Spring Harb. Perspect. Biol.* 10:a032664
112. Shin DH, Brandsen J, Jancarik J, Yokota H, Kim R, Kim SH. 2004. Structural analyses of peptide release factor 1 from *Thermotoga maritima* reveal domain flexibility required for its interaction with the ribosome. *J. Mol. Biol.* 341:227–39
113. Vestergaard B, Van LB, Andersen GR, Nyborg J, Buckingham RH, Kjeldgaard M. 2001. Bacterial polypeptide release factor RF2 is structurally distinct from eukaryotic eRF1. *Mol. Cell* 8:1375–82
114. Demo G, Svidritskiy E, Madireddy R, Diaz-Avalos R, Grant T, et al. 2017. Mechanism of ribosome rescue by ArfA and RF2. *eLife* 6:e23687
115. James NR, Brown A, Gordiyenko Y, Ramakrishnan V. 2016. Translational termination without a stop codon. *Science* 354:1437–40
116. Svidritskiy E, Korostelev AA. 2018. Conformational control of translation termination on the 70S ribosome. *Structure* 26:821–28
117. Trappl K, Joseph S. 2016. Ribosome induces a closed to open conformational change in release factor 1. *J. Mol. Biol.* 428:1333–44
118. Fu Z, Indrisiunaite G, Kaledhonkar S, Shah B, Sun M, et al. 2019. The structural basis for release-factor activation during translation termination revealed by time-resolved cryogenic electron microscopy. *Nat. Commun.* 10:2579
119. Adio S, Sharma H, Senyushkina T, Karki P, Maracci C, et al. 2018. Dynamics of ribosomes and release factors during translation termination in *E. coli*. *eLife* 7:e34252
120. Mikuni O, Ito K, Moffat J, Matsumura K, McCaughan K, et al. 1994. Identification of the prfC gene, which encodes peptide-chain-release factor 3 of *Escherichia coli*. *PNAS* 91:5798–802
121. Grentzmann G, Brechemier-Baey D, Heurgue V, Mora L, Buckingham RH. 1994. Localization and characterization of the gene encoding release factor RF3 in *Escherichia coli*. *PNAS* 91:5848–52
122. Ermolenko DN, Majumdar ZK, Hickerson RP, Spiegel PC, Clegg RM, Noller HF. 2007. Observation of intersubunit movement of the ribosome in solution using FRET. *J. Mol. Biol.* 370:530–40
123. Gao H, Zhou Z, Rawat U, Huang C, Bouakaz L, et al. 2007. RF3 induces ribosomal conformational changes responsible for dissociation of class I release factors. *Cell* 129:929–41
124. Korostelev A, Zhu J, Asahara H, Noller HF. 2010. Recognition of the amber UAG stop codon by release factor RF1. *EMBO J.* 29:2577–85
125. Svidritskiy E, Demo G, Loveland AB, Xu C, Korostelev AA. 2019. Extensive ribosome and RF2 rearrangements during translation termination. *eLife* 8:e46850
126. Graf M, Huter P, Maracci C, Peterek M, Rodnina MV, Wilson DN. 2018. Visualization of translation termination intermediates trapped by the Apidaecin 137 peptide during RF3-mediated recycling of RF1. *Nat. Commun.* 9:3053
127. Fu Z, Kaledhonkar S, Borg A, Sun M, Chen B, et al. 2016. Key intermediates in ribosome recycling visualized by time-resolved cryoelectron microscopy. *Structure* 24:2092–101
128. Brown A, Shao S, Murray J, Hegde RS, Ramakrishnan V. 2015. Structural basis for stop codon recognition in eukaryotes. *Nature* 524:493–96
129. Poole ES, Brown CM, Tate WP. 1995. The identity of the base following the stop codon determines the efficiency of in vivo translational termination in *Escherichia coli*. *EMBO J.* 14:151–58
130. Brown CM, Stockwell PA, Trotman CN, Tate WP. 1990. Sequence analysis suggests that tetranucleotides signal the termination of protein synthesis in eukaryotes. *Nucleic Acids Res.* 18:6339–45
131. Jungreis I, Lin MF, Spokony R, Chan CS, Negre N, et al. 2011. Evidence of abundant stop codon readthrough in *Drosophila* and other metazoa. *Genome Res.* 21:2096–113
132. des Georges A, Hashem Y, Unbehaun A, Grassucci RA, Taylor D, et al. 2014. Structure of the mammalian ribosomal pre-termination complex associated with eRF1•eRF3•GDPNP. *Nucleic Acids Res.* 42:3409–18
133. Preis A, Heuer A, Barrio-Garcia C, Hauser A, Eyler DE, et al. 2014. Cryoelectron microscopic structures of eukaryotic translation termination complexes containing eRF1-eRF3 or eRF1-ABCE1. *Cell Rep.* 8:59–65

134. Pisarev AV, Skabkin MA, Pisareva VP, Skabkina OV, Rakotondrafara AM, et al. 2010. The role of ABCE1 in eukaryotic posttermination ribosomal recycling. *Mol. Cell* 37:196–210
135. Desai BJ, Gonzalez RL Jr. 2020. Multiplexed genomic encoding of non-canonical amino acids for labeling large complexes. *Nat. Chem. Biol.* 16:1129–35
136. Zhong ED, Bepler T, Berger B, Davis JH. 2021. CryoDRGN: reconstruction of heterogeneous cryo-EM structures using neural networks. *Nat. Methods* 18:176–85
137. Schmitt E, Coureux PD, Kazan R, Bourgeois G, Lazennec-Schurdevin C, Mechulam Y. 2020. Recent advances in archaeal translation initiation. *Front. Microbiol.* 11:584152
138. Nurenberg-Goloub E, Kratzat H, Heinemann H, Heuer A, Kotter P, et al. 2020. Molecular analysis of the ribosome recycling factor ABCE1 bound to the 30S post-splitting complex. *EMBO J.* 39:e103788
139. Ranjan N, Pochopien AA, Chih-Chien Wu C, Beckert B, Blanchet S, et al. 2021. Yeast translation elongation factor eEF3 promotes late stages of tRNA translocation. *EMBO J.* 40:e106449
140. Brito Querido J, Sokabe M, Kraatz S, Gordiyenko Y, Skehel JM, et al. 2020. Structure of a human 48S translational initiation complex. *Science* 369:1220–27
141. Aibara S, Singh V, Modelska A, Amunts A. 2020. Structural basis of mitochondrial translation. *eLife* 9:e58362
142. Kummer E, Ban N. 2020. Structural insights into mammalian mitochondrial translation elongation catalyzed by mtEFG1. *EMBO J.* 39:e104820
143. Koripella RK, Sharma MR, Bhargava K, Datta PP, Kaushal PS, et al. 2020. Structures of the human mitochondrial ribosome bound to EF-G1 reveal distinct features of mitochondrial translation elongation. *Nat. Commun.* 11:3830
144. Irastortza-Olaziregi M, Amster-Choder O. 2020. Coupled transcription-translation in prokaryotes: an old couple with new surprises. *Front. Microbiol.* 11:624830
145. Tesina P, Heckel E, Cheng J, Fromont-Racine M, Buschauer R, et al. 2019. Structure of the 80S ribosome–Xrn1 nuclease complex. *Nat. Struct. Mol. Biol.* 26:275–80
146. Matsuo Y, Tesina P, Nakajima S, Mizuno M, Endo A, et al. 2020. RQT complex dissociates ribosomes collided on endogenous RQC substrate SDD1. *Nat. Struct. Mol. Biol.* 27:323–32
147. Demo G, Rasouly A, Vasilyev N, Svetlov V, Loveland AB, et al. 2017. Structure of RNA polymerase bound to ribosomal 30S subunit. *eLife* 6:e28560
148. O'Reilly FJ, Xue L, Graziadei A, Sinn L, Lenz S, et al. 2020. In-cell architecture of an actively transcribing-translating expressome. *Science* 369:554–57
149. Tegunov D, Xue L, Dienemann C, Cramer P, Mahamid J. 2021. Multi-particle cryo-EM refinement with M visualizes ribosome-antibiotic complex at 3.5 Å in cells. *Nat. Methods* 18:186–93
150. Lucas BA, Himes BA, Xue L, Grant T, Mahamid J, Grigorieff N. 2021. Locating macromolecular assemblies in cells by 2D template matching with cisTEM. *eLife* 10:e68946
151. Adio S, Senyushkina T, Peske F, Fischer N, Wintermeyer W, Rodnina MV. 2015. Fluctuations between multiple EF-G-induced chimeric tRNA states during translocation on the ribosome. *Nat. Commun.* 6:7442